Phase aberration simulation study of MRgFUS breast treatments

Alexis I. Farrer,[a] Scott Almquist, Christopher R. Dillon, Leigh A. Neumayer, Dennis L. Parker, Douglas A. Christensen, and Allison Payne
Department of Bioengineering, University of Utah, 36 South Wasatch Drive, Room 3100, Salt Lake City, Utah 84112

(Received 12 November 2015; revised 11 January 2016; accepted for publication 18 January 2016; published 23 February 2016)

Purpose: This simulation study evaluates the effects of phase aberration in breast MR-guided focused ultrasound (MRgFUS) ablation treatments performed with a phased-array transducer positioned laterally to the breast. A quantification of these effects in terms of thermal dose delivery and the potential benefits of phase correction is demonstrated in four heterogeneous breast numerical models.
Methods: To evaluate the effects of varying breast tissue properties on the quality of the focus, four female volunteers with confirmed benign fibroadenomas were imaged using 3T MRI. These images were segmented into numerical models with six tissue types, with each tissue type assigned standard acoustic properties from the literature. Simulations for a single-plane 16-point raster-scan treatment trajectory centered in a fibroadenoma in each modeled breast were performed for a breast-specific MRgFUS system. At each of the 16 points, pressure patterns both with and without applying a phase correction technique were determined with the hybrid-angular spectrum method. Corrected phase patterns were obtained using a simulation-based phase aberration correction technique to adjust each element's transmit phase to obtain maximized constructive interference at the desired focus. Thermal simulations were performed for both the corrected and uncorrected pressure patterns using a finite-difference implementation of the Pennes bioheat equation. The effect of phase correction was evaluated through comparison of thermal dose accumulation both within and outside a defined treatment volume. Treatment results using corrected and uncorrected phase aberration simulations were compared by evaluating the power required to achieve a 20 °C temperature rise at the first treatment location. The extent of the volumes that received a minimum thermal dose of 240 CEM at 43 °C inside the intended treatment volume as well as the volume in the remaining breast tissues was also evaluated in the form of a dose volume ratio (DVR), a DVR percent change between corrected and uncorrected phases, and an additional metric that measured phase spread.
Results: With phase aberration correction applied, there was an improvement in the focus for all breast anatomies as quantified by a reduction in power required (13%–102%) to reach 20 °C when compared to uncorrected simulations. Also, the DVR percent change increased by 5%–77% in seven out of eight cases, indicating an improvement to the treatment as measured by a reduction in thermal dose deposited to the nontreatment tissues. Breast compositions with a higher degree of heterogeneity along the ultrasound beam path showed greater reductions in thermal dose delivered outside of the treatment volume with correction applied than beam trajectories that propagated through more homogeneous breast compositions. An increasing linear trend was observed between the DVR percent change and the phase-spread metric ($R^2 = 0.68$).
Conclusions: These results indicate that performing phase aberration correction for breast MRgFUS treatments is beneficial for the small-aperture transducer (14.4×9.8 cm) evaluated in this work. While all breast anatomies could benefit from phase aberration correction, greater benefits are observed in more heterogeneous anatomies. [http://dx.doi.org/10.1118/1.4941013]

Key words: MRgFUS, phase aberrations, breast heterogeneity, thermal therapies, breast cancer treatments

1. INTRODUCTION

MR-guided focused ultrasound (MRgFUS) has been demonstrated to be potentially effective as a noninvasive breast cancer therapy.[1–13] While most feasibility studies to date have been performed with a vertically propagating transducer, some designs use laterally mounted configurations.[1,13–16] Laterally positioned transducers avoid striking important structures such as the heart, lungs, and ribs in the far field of the beam path when targeting a tumor in the breast, thus reducing reflections and undesired heating in healthy tissues.

One laterally propagating transducer[13–15] has a large-aperture design (270° circular arc surrounding the breast) to decrease the energy deposited in the near field and to reduce skin heating. However, large-aperture phased-array transducers may accentuate phase aberrations since each element's pressure wave must travel through a unique tissue pathway to reach the intended focus. Mougenot *et al.* found that the

beam was indeed aberrated at the intended focus in inhomogeneous phantom experiments for a large-aperture phased-array transducer and therefore recommended phase correction. It remained unknown whether such phase aberrations would be prominent for a treatment using a smaller-aperture transducer.

The breast has a unique structure and composition that varies from individual to individual. According to the American College of Radiology's Breast Imaging Reporting and Data System (BI-RADS),[17] there are four breast density classifications. Large-scale population-based data[18,19] show that the majority of breasts are highly heterogeneous, a mixed composition of breast fat and fibroglandular tissues. It has been noted that the different speeds of sound (c) of these two tissue types ($c_{\text{bfat}} = 1436$ m/s, $c_{fg} = 1514$ m/s)[20] play a prominent role in phase aberrations in the breast[15] during focused ultrasound (FUS) treatments.

The goal of this study is to determine whether phase aberrations would be present for a laterally positioned, small-aperture transducer. This is evaluated through simulating FUS breast treatments in numerical models of breasts with varying degrees of heterogeneity.

2. METHODS

2.A. Simulation geometry

This study simulated ultrasound propagation and focusing in the breasts of four female volunteers using the parameters of a laterally positioned, small-aperture phased-array MRgFUS breast system[16] (Fig. 1). This breast-specific system employs a 256-element, 1-MHz phased-array ultrasound transducer whose 4-mm diameter elements are randomly positioned over a spherical surface with a 10-cm radius of curvature and a 14.4×9.8-cm aperture (Imasonic, Voray-sur-l'Ognon, France).[16] It is driven by electronics developed by Image Guided Therapy (Pessac, France), with a beam full-width half-maximum (FWHM) of $1.8 \times 2.4 \times 8.0$ mm^3 as measured by hydrophone in water. The ultrasound transducer is mounted laterally on a treatment cylinder that can rotate freely under the patient, allowing for multiple acoustic window sites and providing a large treatment volume (TV).

2.B. Subject selection

For the images used in this simulation study, four female volunteers with biopsy confirmed fibroadenomas were selected based on the criterion that they fit on the MRgFUS breast system's patient table inside of the bore of the MRI scanner (49-cm wide table, 60-cm wide MRI bore). The volunteers ranged in age from 18 to 45 and had at least one confirmed fibroadenoma, with two volunteers having multiple fibroadenomas (up to eight). All procedures were performed with Institutional Review Board approval.

2.C. MR data acquisition

All imaging was performed with the system inside a Siemens TIM Trio 3T MRI scanner. The system has a custom integrated 11-channel radio frequency (RF) coil to provide improved SNR for treatment planning, monitoring and assessment.[21] To identify the different tissue types in the breast anatomy, several image contrasts were obtained. These included a three-point Dixon 3D gradient echo (GRE) acquisition with $TR/TE = 11/2.6$, 3.65, 4.6 ms, and $FA = 25°$, and a 3D T1weighted (T1w) VIBE with $TR/TE = 4.91/1.97$ ms and FA = 9°. All scans had FOV = $192 \times 192 \times 120$ mm, were acquired at 1-mm isotropic resolution, and then zero-filled interpolated to 0.5-mm isotropic. Gadolinium contrast was also used for all four volunteers to better identify the fibroadenomas. A central slice of the contrast-enhanced T1w images through the targeted fibroadenoma for each volunteer is shown in Fig. 2.

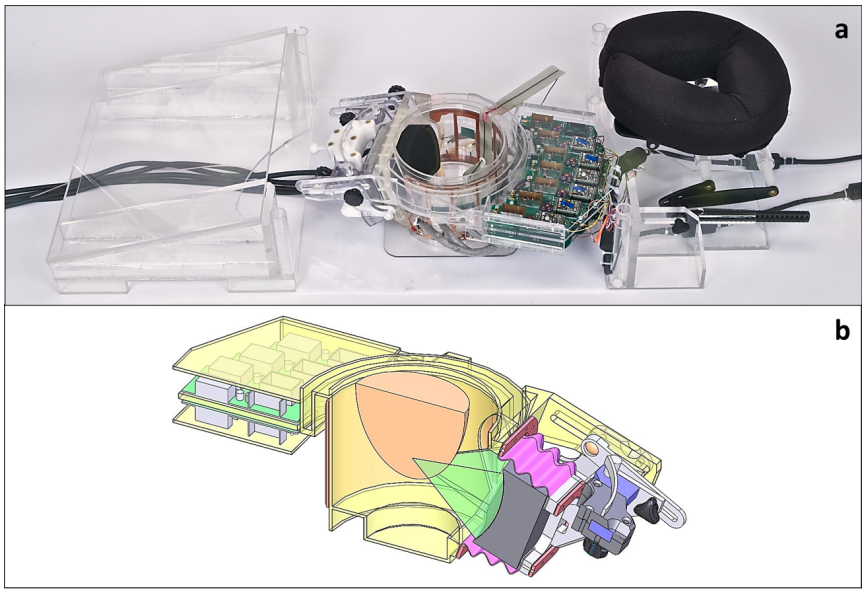

FIG. 1. MRgFUS breast treatment system used in all simulations shown (a) without the treatment table and (b) as a SOLIDWORKS CAD drawing cut-away.

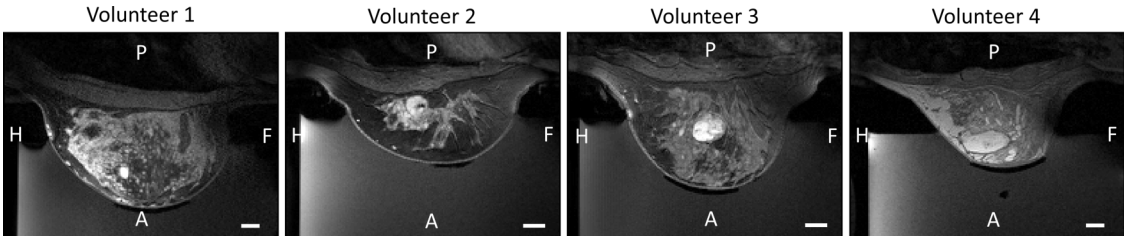

FIG. 2. Contrast-enhanced T1w MR images of all four volunteers (sagittal view) that demonstrate the varied breast heterogeneities. White scale bar represents 1 cm. *P* = posterior; *A* = anterior; *H* = head; *F* = foot.

2.D. Segmentation

The MR images were segmented into numerical models with six tissue/material types (water, skin, breast fat, fibroglandular tissue, fibroadenoma, and a silicone-rubber nipple cover). The semiautomatic algorithm was performed using the following steps: (1) The three-point Dixon images were used to segment the breast into fat and water-based tissues. (2) The skin was segmented using an edge detection algorithm and was assigned a set thickness (1.5 mm). (3) Water-based tissues inside the skin boundary were identified as fibroglandular tissue while water-based voxels outside the skin were segmented as water. (4) The nipple cover was segmented using a mask, since the size and shape of the nipple cover was known. (5) The fibroadenomas were manually segmented using the contrast-enhanced T1w images. Figure 3 shows the segmented models for each of the four volunteers in the same slices as shown in Fig. 2.

2.E. Treatment strategy

Although some breast models had multiple fibroadenomas, only one fibroadenoma per breast model was simulated for treatment. The selected lesion was at least 1 cm from the skin and 1 cm from the chest wall. Also, when multiple lesions were available for selection, fibroadenomas located in the middle of the breast were selected for the simulated treatments. Three of the four volunteers met these selection criteria. In Volunteer 4, the fibroadenoma was less than 1 cm from the skin. However, while the fibroadenoma itself did not meet the 1-cm distance from skin requirement, the region targeted during simulation in this large fibroadenoma was located 1-cm from the skin.

Because the breast MRgFUS system design used in these simulations[16] allows for multiple directional approaches, one superior (head to foot) and one inferior (foot to head) approach were selected for each breast model, with both approaches targeting the same treatment voxels in the fibroadenoma. Both approaches had the same angle to the horizontal and were rotated 180° around the breast. An example of these approaches for Volunteer 2 is shown in Fig. 4, where the transducer beam is indicated by the blue dotted outline. Figure 4 also shows viewing Planes 1 and 2. Plane 1 represents the slice orientation for an oblique coronal view with respect to the transducer, while Plane 2 represents the slice orientation for an oblique axial view.

In order to obtain a direct comparison of the potential phase aberration effects, a single-plane 16-point raster-scan treatment trajectory (2-mm spacing between points) was centered in the fibroadenoma in each modeled breast. This trajectory was not designed to ablate the entire fibroadenoma volume but to enable systematic testing of potential aberrations that could occur during a treatment. Since the fibroadenomas varied in size, a consistent treatment volume was selected for comparison between breast models. A TV was defined as 150% of the power density's FWHM of the combined, simulated 16 focal spots ($10 \times 10 \times 12$ mm^3) and is used for comparison throughout this work. Figure 5 shows a schematic of the selected 16-point treatment trajectory viewed in both Planes 1 and 2 for Volunteer 2, inferior approach, and defines the treatment volume (box outlined in white). The treatment volume is the same size for all breast models and approaches.

2.F. Ultrasound simulations

Each tissue type was assigned nominal acoustic properties from the literature[20] (see Table I). A through-transmission technique[26,27] was employed to find the speed of sound and attenuation coefficient for the silicone-rubber nipple cover, and its density was found using displaced volume and weighed mass.

The 3D pressure and power deposition patterns for all four models and both approaches were calculated using the hybrid-angular spectrum (HAS) method.[28] The HAS technique is a

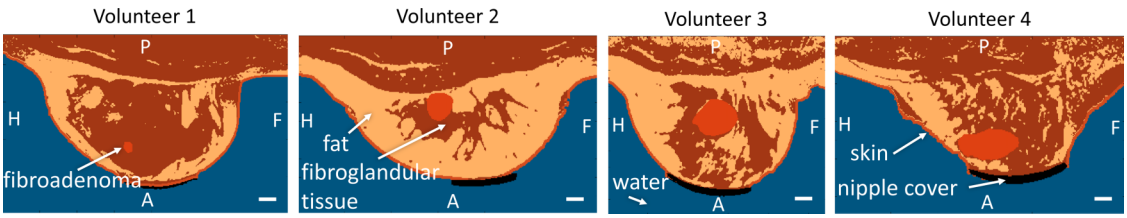

FIG. 3. Images segmented into six tissue/material types: water, skin, fibroglandular tissue, breast fat, fibroadenoma, and silicone rubber (nipple cover). The same sagittal slices are shown here as shown in Fig. 2. White scale bar represents 1 cm. *P* = posterior; *A* = anterior; *H* = head; *F* = foot.

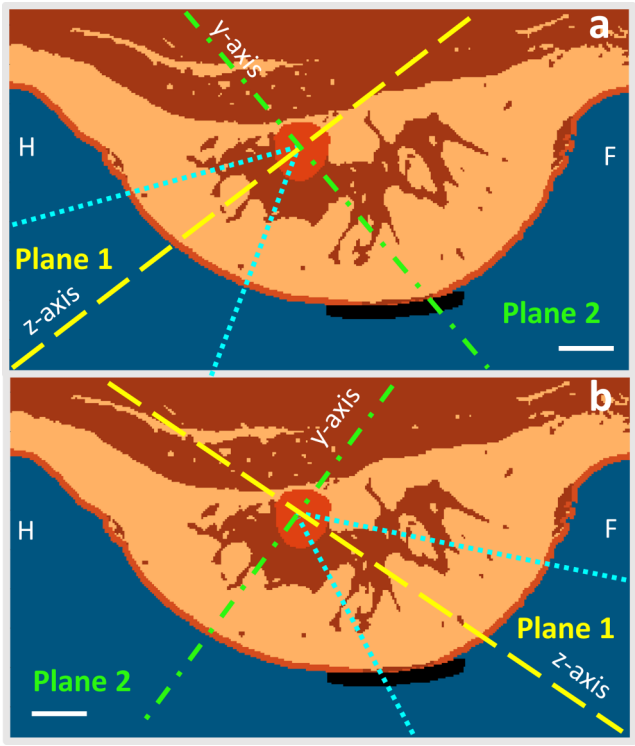

FIG. 4. Two simulated approaches shown for Volunteer 2: (a) superior approach (head to foot) where the transducer is to the bottom-left (not shown) and (b) inferior approach (foot to head) where the transducer is to the bottom-right (not shown). Also shown are the oblique planes used to view the simulation results: Plane 1 is the oblique coronal view (yellow dashed line) which contains the z-axis of our ultrasound simulation coordinate system, and Plane 2 is the oblique axial view (green dashed-dotted line) which contains the y-axis; both are centered in the lesion. The images shown are in planes perpendicular to the x-axis. The width of the ultrasound beam is shown in dotted blue. White scale bar represents 1 cm. H = head; F = foot.

rapid and efficient method that initially imports a precomputed file of the pressures from each element of the transducer to the front plane of the numerical model. This source file needs to be computed only once for a given transducer using the Rayleigh-Sommerfeld integral and is adjusted for each sonication to steer the beam to the intended focal point. The HAS approach then computes the 3D ultrasound pressure patterns by alternating between the space and spatial-frequency domains throughout the inhomogeneous model volume using MATLAB's fft and ifft functions. The technique accounts for beam refraction, absorption, and first-order reflections.[28] The HAS method assumes linear propagation only; nonlinear effects were neglected since the peak simulated pressure levels were moderate (approximately 5 MPa). The HAS software was used to quickly acquire the full 3D pressure and power deposition patterns for each treatment location simulated (on the order of 10 s for each location).

2.G. Phase correction technique

The simulation-based phase aberration correction technique was performed for each sonication point as follows: HAS simulations were used to calculate the 3D pressure patterns from each of the 256 phased-array elements, assuming zero phase and uniform amplitude. Because the pressure patterns extended over the entire volume of the breast model, the inverse of the calculated phases at any desired focal point could be imposed on the respective elements upon transmit. This allowed for maximum constructive interference at the desired focus, effectively correcting for the aberrations due to the initial phase offsets.[29] This calculation was performed efficiently through parallelizing the computation on an Nvidia Tesla GPU (Nvidia, Santa Clara, CA, USA).

2.H. Straight-line ray-trace simulations

To evaluate whether a simple and rapid geometric test could be used to predict the need for phase correction, a straight-line ray-trace method was implemented as a computationally fast method to determine the approximate spread of phases at the geometric focus. The method traces a straight line from the transducer's geometric focal location back to the center

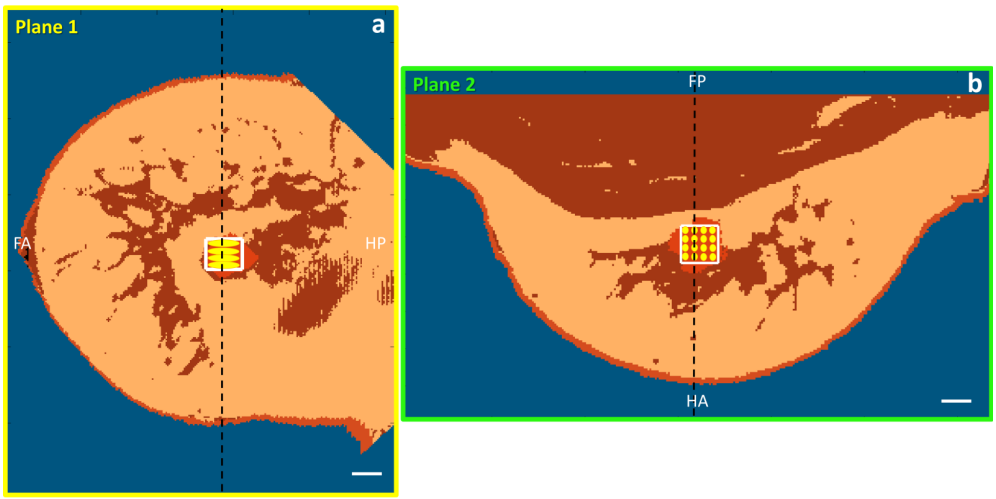

FIG. 5. The 16-point trajectory for Volunteer 2 with the intended TV outlined in white for both (a) Plane 1 (oblique coronal slice centered in lesion; transducer is to the left, not shown) and (b) Plane 2 (oblique axial slice centered in lesion; transducer is in front of the image, not shown). The dashed black line represents the slice location of the orthogonal plane. White scale bar represents 1 cm. *FA* = foot/anterior; *HP* = head/posterior; *HA* = head/anterior; *FP* = foot/posterior.

TABLE I. Acoustic and thermal tissue and material properties used in the simulations.

	Speed of sound (m/s)	Attenuation (dB/cm/MHz)	Density (kg/m^3)	Thermal conductivity (W/m/K)	Specific heat capacity (J/kg/°C)	Perfusion/heat transfer rate (kg/m^3/s)
Water	1500 (Ref. 20)	0 (Ref. 20)	1000 (Ref. 20)	0.58 (Ref. 22)	4182 (Ref. 20)	0[a]
Skin	1537 (Ref. 20)	0.028 (Ref. 20)	1100 (Ref. 20)	0.37 (Ref. 23)	3391 (Ref. 23)	1.77 (Ref. 23)
Fibroglandular tissue	1514 (Ref. 20)	0.090 (Ref. 20)	1058 (Ref. 20)	0.33 (Ref. 23)	2960 (Ref. 23)	2.50 (Ref. 23)
Breast fat	1436 (Ref. 20)	0.070 (Ref. 20)	928 (Ref. 20)	0.21 (Ref. 23)	2348 (Ref. 23)	0.78 (Ref. 23)
Fibroadenoma/tumor	1584 (Ref. 20)	0.081 (Ref. 20)	1041 (Ref. 20)	0.56 (Ref. 20)	3600[a]	10 (Ref. 24)
Silicone rubber (nipple cover)	1480[b]	0.086[b]	937[c]	0.15 (Ref. 22)	1175 (Ref. 25)	0[a]

[a]Likely value (no reference available).
[b]Through-transmission measurement.
[c]Volume displacement technique.

of each of the 256 elements of the transducer. The phase (φ_n) that accumulates due to sound velocity variation along each straight-line path was summed for all 256 straight-line rays (N) using phasor addition and normalized to determine a phase metric value to quantify the phase spread, given by the following:

$$\text{phase spread metric} = 1 - \frac{\sum_{n=1}^{N} 1 \cdot e^{j\varphi_n}}{N}. \quad (1)$$

Using Eq. (1), a value of 0 represents a tightly focused case with no phase spread and 1 denotes full phase spread. Additionally, the straight-line ray-trace algorithm was used to calculate the average tissue path length that the rays pass through, the average total accumulation of pressure reflection coefficient for the rays, and the average number of tissue interfaces that the rays pass through before reaching the intended focus.

2.I. Thermal simulations

Thermal simulations were performed for both the corrected and uncorrected pressure patterns using a finite-difference implementation[30] of the Pennes bioheat equation,[31]

$$\rho_t c_t \frac{dT(x,y,z,t)}{dt} = Q_a(x,y,z,t) + k_t \nabla^2 T - w_b(c_t T - c_b T_b), \quad (2)$$

where T is the tissue temperature in °C; x, y, z are the spatial coordinates in m; t is time in s; ρ_t is the tissue density in kg/m^3; c_t and c_b are the tissue's and blood's specific heat capacities, respectively, in J/kg/°C (we assumed that the specific heat of the blood and the tissue is equal); Q_a is the absorbed ultrasound power per unit volume in W/m^3; k_t is the tissue's thermal conductivity in W/m/°C; w_b is the blood perfusion rate in kg/m^3/s; and T_b is the temperature of the blood in °C. T_b and all boundaries were held constant at the tissue's initial temperature of 37 °C. The thermal conductivity, specific heat capacity, and perfusion flow rates used for each tissue/material type are provided in Table I.

The ultrasound power applied for each breast model and approach combination was determined by finding the power required to produce a 20 °C temperature rise in 15 s at the first treatment location. (However, for Volunteer 3, inferior approach, the first treatment location of the trajectory fell outside of the fibroadenoma. Therefore, the applied power was adjusted based on the 16th treatment location for this case only.) Using this identified power level, a treatment was simulated that consecutively heated each of the 16 locations for 15 s with no cooling between points. This treatment was designed to maximize any potential thermal accumulation in the near field and minimize cooling effects in the treatment volume to emphasize potential effects of phase aberration on the overall treatment. Two minutes of cooling were simulated at the end of each treatment to capture any accumulation of thermal dose that occurs during the cooling phase. Thermal effects of the nipple cover were neglected in the simulations. While the nominal fibroadenoma perfusion was set to 10 kg/m^3/s, perfusion values of 1.0, 2.5, and 5.0 kg/m^3/s (Ref. 32) were also studied for one case (Volunteer 2, inferior approach) to better elucidate what effects perfusion of the fibroadenoma had on the overall treatment, both with and without phase correction.

The accumulated thermal dose, measured in cumulative equivalent minutes at 43 °C (CEM at 43 °C), was calculated throughout the entire volume for a full 16-point treatment simulation, using the following formulation:[33]

$$\text{CEM at } 43\,^\circ\text{C} = \int_0^t R^{T-43} dt, \quad (3)$$

where t is the time in min, T is the temperature in °C, and $R = 2$ when $T \geq 43$ °C or $R = 4$ when $T \leq 43$ °C.

In addition, a metric was calculated to quantify the volume that was treated at or above 240 CEM at 43 °C for use in comparing the treatment with and without phase correction. This metric, the dose volume ratio (DVR), is defined by

$$\text{DVR} = \frac{\text{volume inside TV} \geq 240 \text{ CEM at } 43\,^\circ\text{C}}{(\text{volume outside TV} + \text{volume inside TV}) \geq 240 \text{ CEM at } 43\,^\circ\text{C}}, \quad (4)$$

where TV is the treatment volume as shown in Fig. 5. With this definition, the DVR can range from 0 to 1, with the limits indicating that all dose >240 CEM at 43 °C falls outside or inside the treatment volume, respectively.

The change in DVR and acoustic power needed to reach 20 °C temperature rise at the first treatment location due to phase correction is found using the following equation:

$$\%\ \text{change} = \frac{(\text{corrected} - \text{uncorrected})}{\text{corrected}} \times 100. \quad (5)$$

This was calculated to illustrate the improvement that phase correction had in decreasing the amount of applied power as well as the amount of volume outside the TV that was dosed at or above 240 CEM at 43 °C.

2.J. Tissue heterogeneity

To assess whether phase aberration correction in the treatment planning stage would be beneficial for more homogeneous breast anatomies, one breast model was numerically altered (Volunteer 2) to create both an all-fibroglandular tissue model and an all-breast-fat model, with the fibroadenoma left in place, representing the two extreme homogeneous anatomy cases. Selecting only the inferior approach, full acoustic and thermal simulations were run for the 16-point treatment trajectory in the fibroadenoma for both artificially altered breasts models. In addition, in order to determine the effect of the nipple cover on phase aberrations, a limited number of acoustic simulations were run both with and without the nipple cover in place.

3. RESULTS

The power required to achieve a 20 °C temperature rise at the first treatment location in both corrected and uncorrected phase aberration treatment simulations is reported in Table II. In all simulated cases, less power was needed to achieve the same temperature rise with phase correction applied, with a range of 13%–102% reduction in power required. The DVRs [Eq. (4)] and the DVR percent change [Eq. (5)] for all cases are provided in Table II. For seven out of eight of the breast simulations, the DVR percent change was positive, indicating an increase in the DVR value once phase correction was applied. Also, using the ray-trace algorithm, the average length of tissue propagated through, the average total pressure reflection coefficient, the average number of interfaces passed through, and the phase-spread metric [Eq. (1)] are also shown in Table II to indicate their correlation to the degree of improvement that the phase correction had for each model and approach. In comparing simulations run with and without the nipple cover in place, there was no noticeable difference in the beam pressure results indicating the nipple cover has little to no effect on beam aberration.

Figures 6–9 show thermal dose maps in Plane 1 (Fig. 4, oblique coronal) for Volunteers 1–4, respectively. (a) and (c) show no phase correction applied and (b) and (d) show the same region with phase aberration correction applied.

TABLE II. Summary of simulated phase correction results in terms of reduced acoustic power and increased DVR for two approaches for each volunteer, as well as two artificially modified treatments representing extremes of homogeneous fat and homogeneous glandular tissue.

		Acoustic power (W) needed to reach 20 °C			Dose volume ratio (DVR)			Straight-line ray-trace calculations			
		Uncorrected phases	Phase correction applied	% change	Uncorrected phases	Phase correction applied	% change	Average tissue path length (mm)	Average total reflection coefficient (%)	Average number of interfaces passed through	Phase spread metric
Volunteer 1	Sup.	4.2	3.6	−17	0.91	0.96	+5	32	2.6	7.6	0.08
	Inf.	6.0	4.8	−25	0.89	0.95	+6	45	4.6	7.9	0.46
Volunteer 2	Sup.	6.6	5.7	−16	0.37	0.42	+11	42	2.6	7.7	0.23
	Inf.	18.2	9.5	−92	0.10	0.20	+51	63	2.4	12.0	0.82
Volunteer 3	Sup.	9.9	7.3	−36	0.45	0.68	+34	40	6.0	8.9	0.40
	Inf.[a]	23.8	11.8	−102	0.08	0.34	+77	61	18.0	14.0	0.68
Volunteer 4	Sup.	5.4	4.5	−20	0.36	0.31	−15	20	2.7	6.9	0.06
	Inf.	6.3	5.6	−13	0.23	0.33	+29	41	7.4	12.0	0.27
Artificial model	Fat homg.	10.5	7.6	−38	0.26	0.20	−31	63	1.3	2	0.43
(Volunteer 2, inf.)	Glnd. homg.	11.7	9.5	−23	0.47	0.40	−17	63	0.7	2	0.05

[a]Power calibrated to 16th treatment location because the first treatment location was outside of the small fibroadenoma; Sup. = superior approach; Inf. = inferior approach; Homg. = homogeneous; Glnd. = fibroglandular tissue.

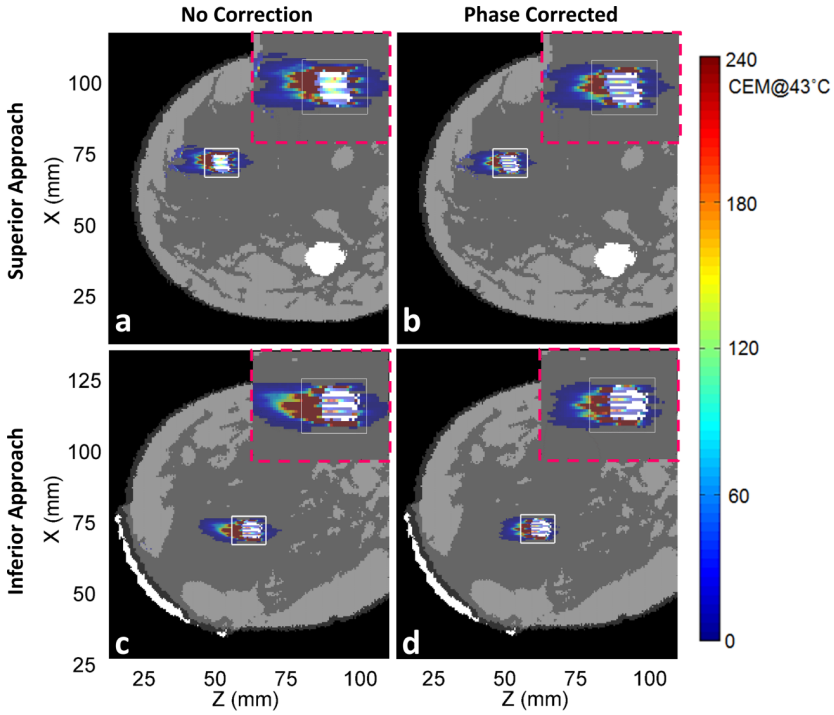

FIG. 6. Simulated results for Volunteer 1 for the full 16-point trajectory thermal dose accumulation throughout the entire breast volume in Plane 1 in which (a) and (b) show the superior approach treatment and where (c) and (d) show the inferior approach. (a) and (c) show the results without phase correction applied and (b) and (d) with phase correction applied. Also, a zoomed-in portion of the TV region is shown in the upper right-hand corner (pink-dashed outline) of its corresponding thermal dose map. The transducer is to the horizontal left of all images (not shown). See Fig. 4 for definition of x, y, and z coordinate system.

The superior approach of beam propagation through the model is shown in (a) and (b), while the inferior approach is shown in (c) and (d). A zoomed-in region of the TV is shown for each case in the upper right-hand corner (pink-dashed outline) of each thermal dose map. A decrease in thermal dose accumulation was seen throughout the entire breast volume in all examples after phase correction was applied.

Table III shows the effects of varying the fibroadenoma perfusion rate on the thermal dose patterns for Volunteer 2, inferior approach. Increasing the perfusion rate increased

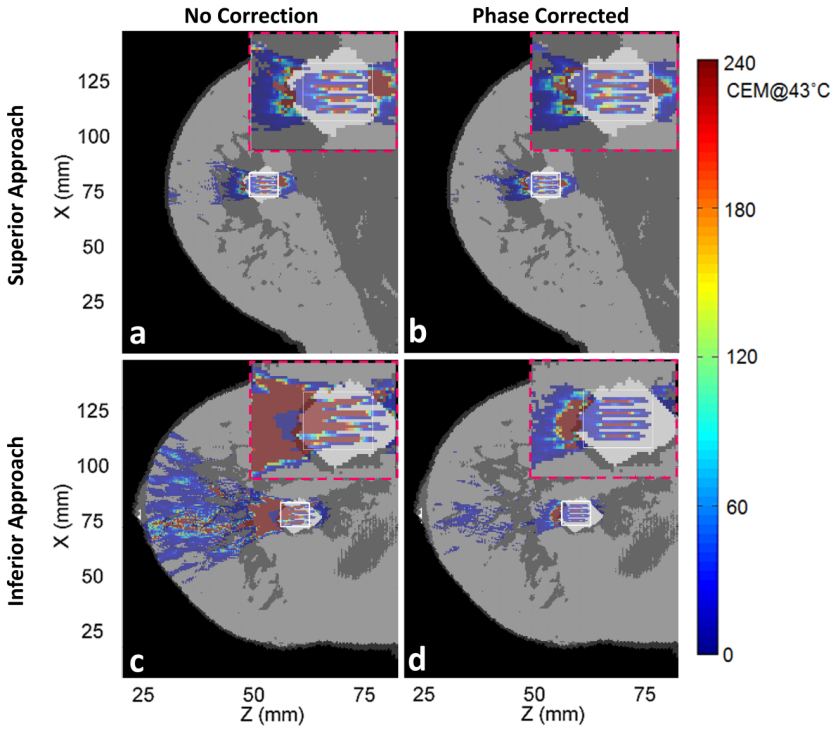

FIG. 7. Simulated thermal dose patterns in the same views as in Fig. 6, for Volunteer 2.

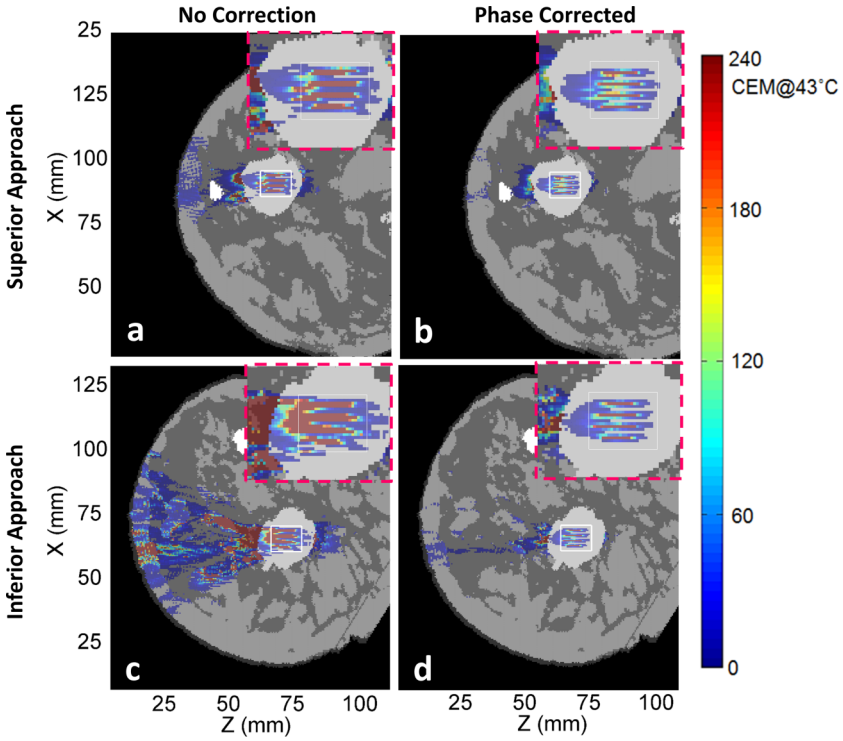

FIG. 8. Simulated thermal dose patterns in the same views as in Fig. 6, for Volunteer 3.

the power required to reach 20 °C as well as decreased the DVR for both the uncorrected and phase corrected cases. The required power decreased by about 92% with phase correction for all four of the perfusion cases.

Figure 10 shows a scatterplot of the percent change in DVR as a function of the phase-spread metric found from the straight-line ray-trace method for all four breast models for both superior and inferior approaches ($n = 8$). Each point is labeled with its corresponding volunteer number as well as the approach direction. An increasing relationship between the phase-spread metric and the percent change in DVR is observed in Fig. 10 with a least squares linear fit (R^2) value of 0.68.

4. DISCUSSION

The main objective of this study was to determine whether significant phase aberrations were present for a breast-specific MRgFUS system with a small-aperture transducer, and if phase aberration correction would benefit treatments. A

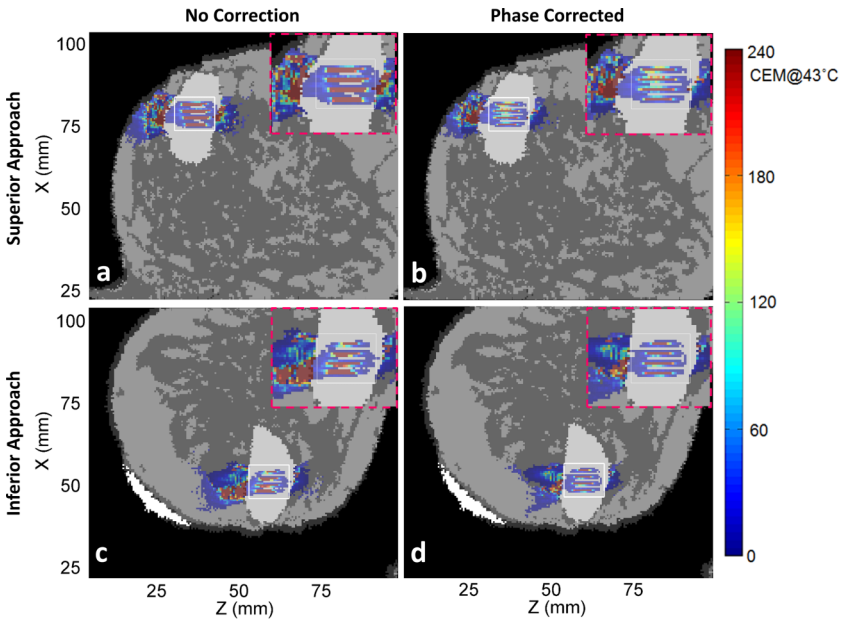

FIG. 9. Simulated thermal dose patterns in the same views as in Fig. 6, for Volunteer 4.

TABLE III. The effects of treatment on the Volunteer 2 model, inferior approach, for varying fibroadenoma perfusion flow rates.

Perfusion rates (Volunteer 2, inferior approach) ($kg/m^3/s$)	Acoustic power (W) needed to reach 20 °C			Dose volume ratio (DVR)		
	Uncorrected phases	Phase correction applied	% change	Uncorrected phases	Phase correction applied	% change
1.0	17.2	8.9	−93	0.22	0.58	+61
2.5	17.3	9.0	−92	0.19	0.41	+53
5.0	17.6	9.2	−91	0.14	0.26	+47
10.0	18.2	9.5	−92	0.10	0.20	+51

secondary objective was to derive a metric that could indicate when phase correction would be beneficial in a treatment planning capacity for a specific breast anatomy by investigating the role that tissue heterogeneity along the beam path has on the degree of improvement with phase aberration correction employed without cooling between sonication locations (worst-case scenario).

Phase aberration correction improved almost all of the treatments for our small-aperture breast-specific system. The applied acoustic power was decreased in all cases after phase correction. Near-field heating effects, the thermal dose accumulation in the near-field regions outside of the TV (shown with the white outlined box in Figs. 5–9), decreased for all eight cases when aberration correction was applied. This was particularly evident for Volunteers 2 and 3, inferior approach, in which the beam path can qualitatively be seen to pass through more tissue interfaces before reaching the TV.

For all simulations except one (Volunteer 4, superior approach), the DVR increased with phase correction, leading to a desirable positive percent change in DVR. The percent change in DVR was modest in three of these cases (below 15%), indicating a small improvement with phase correction: Volunteer 1, both superior and inferior approaches, and Volunteer 2, superior approach. For these cases, the fibroadenomas were close in volume with and had more homogeneous paths to the TV and had fibroglandular tissue in the direct near-field path to the fibroadenoma. Since DVR is directly calculated using thermal dose and because fibroglandular tissue has a higher thermal conductivity and perfusion value than breast fat, less thermal dose accrues in these regions when compared with anatomies with primarily breast fat in the intervening tissues. Two cases had a more notable change in DVR (approximately 30%): Volunteer 3, superior approach, and Volunteer 4, inferior approach. For these cases, the fibroadenomas were much larger than the TV and the beam path in the direct near field of the fibroadenoma changed several times between fat and fibroglandular tissue before reaching the fibroadenoma (see Table II). Most significant were the two cases above 50% improvement, signifying a large benefit with phase correction applied: Volunteer 2, inferior approach, and Volunteer 3, inferior approach. In these two cases, the ultrasound also passed through many tissue interfaces due to the high heterogeneity along the beam path, as well as having a longer path of propagation before reaching the fibroadenoma.

The one case with the negative percent change in DVR was the superior approach for Volunteer 4, where the fibroadenoma was directly adjacent to the skin. The superior approach path traveled through the least amount of tissue and passed through a fairly homogeneous tissue region with the fewest number of tissue interfaces when compared to the other models. The TV for Volunteer 4 fell completely within the fibroadenoma. With phase correction applied, the DVR decreased because even though the amount of treated volume outside of the TV was reduced, the amount of treated volume within the TV was reduced by a larger ratio. Phase correction improved the tightness of the focus, decreasing the more broad focus that occurred with uncorrected phases. Since the fibroadenomas were set with high perfusion values, a

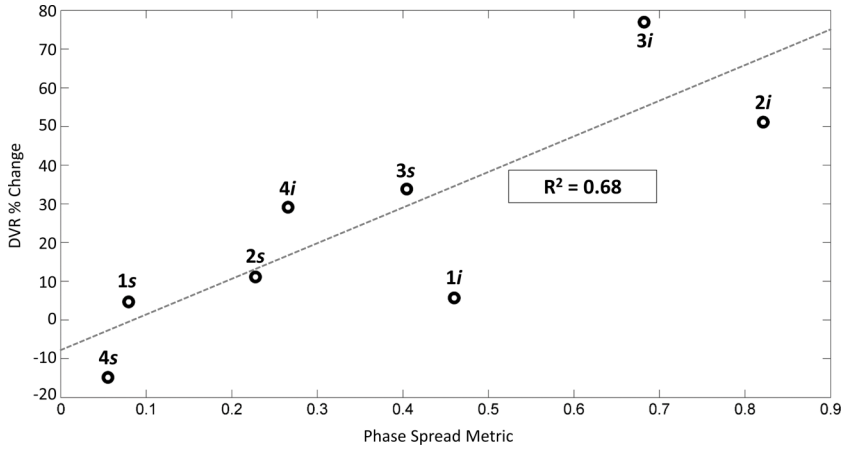

FIG. 10. The percent change in DVR [Eq. (5)] plotted with the corresponding change in phase-spread metric [Eq. (1)] for each of the four breast anatomies for both the superior and inferior approaches. Each point is labeled with its corresponding volunteer number (1–4) and approach direction (*s* for superior; *i* for inferior). Least squares linear fit value is shown as R^2.

tighter focus led to a more precise heated focal location for all 16 sonication points in the treatment, decreasing the amount of volume treated within the TV region. Therefore, even though the percent change in DVR was negative, this treatment showed improvement when phase corrected as judged by a 17% decrease in power required and tighter foci, shown by comparing the zoomed-in regions of Figs. 9(b) to 9(a).

As expected, the impact of increased perfusion in the treated fibroadenoma required an increased transducer power output to achieve a 20 °C rise at the first sonication point, as shown in Table III. The power output increased from 17.2 W at a flow rate of 1.0 kg/m^3/s to 18.2 W at a flow rate of 10.0 kg/m^3/s. This approximately 5% increase of power was similar to results shown by Billard *et al.*,[34] who demonstrated that the peak temperature decreases by less than 10% with a perfusion increase from 0 to 10 kg/m^3/s. The percent of change in DVR decreased modestly with increasing perfusion rate (from 61% at 1.0 kg/m^3/s to 51% at 10.0 kg/m^3/s). The perfusion increase in the tumor results in a decreased ability to treat the target but does not affect the heating in the near-field, thus reducing the effectiveness of phase aberration correction as assessed by the DVR metric.

While the number of anatomies presented in this study is limited, the presented data suggest that the treatments that benefited the most from phase aberration correction were when the average tissue length propagated through was greater than 40 mm, the average total reflection coefficient was above 5%, more than eight average tissue interfaces were passed through, and the spread of phase value was greater than 0.7. Breast anatomies that have a combination of at least three of these four rough estimated requirements seem indicative that they will yield a percent change in DVR of about 30% or more, which supports a case where applying phase correction will considerably benefit the FUS treatment.

The results presented in this work are consistent with what has been observed clinically. Deckers *et al.* treated ten females with invasive breast cancer using a dedicated large-aperture phased-array laterally shooting MRgFUS therapy system. They did not use a phase aberration correction method, yet reported sonications that were accurate in positioning to about 2 mm. However, they stated that the patients' breast anatomies were almost entirely fatty. Also, although they qualitatively accessed the skin for burns, there was no monitoring of near-field heating. Similarly, we also found in the artificial homogeneous models studied in this work (Table II) that phase aberration correction does not demonstrate notable benefits. Since the more heterogeneity present in the breast seemed to be a qualitative indicator that phase aberrations were more pronounced, we expected very little phase distortion of the focal regions in these extreme homogeneous models. Our results based on the negative DVR values (−31% for all breast fat model; −17% for all fibroglandular tissue model) indicated that the phase aberration correction was not beneficial for these extreme homogeneous breast anatomy cases.

Mougenot *et al.* noted that the varying speed of sounds of the tissues in the breast played a prominent role in phase aberrations that led to a broadening of the pressure pattern at the focus. As demonstrated in this study, the treatments that benefited the most from phase aberration correction (Volunteers 2 and 3, both inferior approaches) had more heterogeneity along the beam path, in which the ultrasound waves passed through breast fat and fibroglandular tissue multiple times before reaching the TV region inside the fibroadenoma.

The most consistent benefit of applying a phase aberration correction to the treatment is the reduction in the power required from the transducer. Reducing the energy deposited in the near field as well as potentially reducing the overall treatment time by decreasing the cooling periods needed between sonications would potentially make MRgFUS breast treatments more efficient and possibly reduce unwanted complications. However, to reduce near-field heating without applying a phase correction, cooling times between each sonication can be implemented. This would help to achieve a DVR value closer to one without applying a phase correction technique at the cost of increasing the overall treatment time. Wu *et al.* treated 22 breast cancer patients using MRgFUS without applying a phase correction and reported that local mammary edema was present immediately following the treatment, but gradually disappeared over the course of several postoperative weeks. This was also found in the work of Payne *et al.* in *in vivo* goat udder models. While these results were not directly related to transducer power output, it is possible that improving the focus and reducing near-field heating through applying phase aberration correction could potentially reduce the overall treatment time for MRgFUS breast cancer therapy, justifying the time added to the treatment planning stage for phase aberration correction.

5. CONCLUSIONS

The objective of this work was to assess whether significant phase aberrations would be present for a small-aperture laterally positioned breast-specific phased-array transducer. Our findings were that phase aberrations were present, but only notably for more heterogeneous beam path trajectories. Phase aberration correction improved the majority of treatments; however, the degree of improvement was dependent on multiple factors: average tissue length of beam propagation, average total reflection coefficients, average number of interfaces passed through by the ultrasound beam, the spread of the phases at the geometric focus, and the rate of perfusion of the tissue type at the intended sonication points.

ACKNOWLEDGMENTS

The authors thank Dr. Joshua de Bever for his coding consultations and Heather McLean and Chad Duncan for the manual segmentation of the fibroadenomas. The authors acknowledge support from Siemens Healthcare AG, the FUS Foundation, and NIH Grant No. RO1 CA172787.

[a]Author to whom correspondence should be addressed. Electronic mail: alexis.farrer@utah.edu

[1]P. E. Huber, J. W. Jenne, R. Rastert, I. Simiantonakis, H. P. Sinn, H. J. Strittmatter, D. von Fournier, M. F. Wannenmacher, and J. Debus, "A new noninvasive approach in breast cancer therapy using magnetic

resonance imaging-guided focused ultrasound surgery," Cancer Res. **61**(23), 8441–8447 (2001).
[2]K. Hynynen, O. Pomeroy, D. N. Smith, P. E. Huber, N. J. McDannold, J. Kettenbach, J. Baum, S. Singer, and F. A. Jolesz, "MR imaging-guided focused ultrasound surgery of fibroadenomas in the breast: A feasibility study," Radiology **219**(1), 176–185 (2001).
[3]D. Gianfelice, A. Khiat, M. Amara, A. Belblidia, and Y. Boulanger, "MR imaging-guided focused US ablation of breast cancer: Histopathologic assessment of effectiveness–initial experience," Radiology **227**(3), 849–855 (2003).
[4]D. Gianfelice, A. Khiat, Y. Boulanger, M. Amara, and A. Belblidia, "Feasibility of magnetic resonance imaging-guided focused ultrasound surgery as an adjunct to tamoxifen therapy in high-risk surgical patients with breast carcinoma," J. Vasc. Interventional Radiol. **14**(10), 1275–1282 (2003).
[5]F. Wu, Z. B. Wang, Y. D. Cao, W. Z. Chen, J. Z. Zou, J. Bai, H. Zhu, K. Q. Li, C. B. Jin, F. L. Xie, H. B. Su, and G. W. Gao, "Changes in biologic characteristics of breast cancer treated with high-intensity focused ultrasound," Ultrasound Med. Biol. **29**(10), 1487–1492 (2003).
[6]F. Wu, Z. B. Wang, H. Zhu, W. Z. Chen, J. Z. Zou, J. Bai, K. Q. Li, C. B. Jin, F. L. Xie, and H. B. Su, "Extracorporeal high intensity focused ultrasound treatment for patients with breast cancer," Breast Cancer Res. Treat. **92**(1), 51–60 (2005).
[7]D. B. Zippel and M. Z. Papa, "The use of MR imaging guided focused ultrasound in breast cancer patients; a preliminary phase one study and review," Breast Cancer **12**(1), 32–38 (2005).
[8]H. Furusawa, K. Namba, S. Thomsen, F. Akiyama, A. Bendet, C. Tanaka, Y. Yasuda, and H. Nakahara, "Magnetic resonance-guided focused ultrasound surgery of breast cancer: Reliability and effectiveness," J. Am. Coll. Surg. **203**(1), 54–63 (2006).
[9]H. Furusawa, K. Namba, H. Nakahara, C. Tanaka, Y. Yasuda, E. Hirabara, M. Imahariyama, and K. Komaki, "The evolving non-surgical ablation of breast cancer: MR guided focused ultrasound (MRgFUS)," Breast Cancer **14**(1), 55–58 (2007).
[10]A. Khiat, D. Gianfelice, M. Amara, and Y. Boulanger, "Influence of post-treatment delay on the evaluation of the response to focused ultrasound surgery of breast cancer by dynamic contrast enhanced MRI," Br. J. Radiol. **79**(940), 308–314 (2006).
[11]A. C. Schmitz, D. Gianfelice, B. L. Daniel, W. P. Mali, and M. A. van den Bosch, "Image-guided focused ultrasound ablation of breast cancer: Current status, challenges, and future directions," Eur. Radiol **18**, 1431–1441 (2008).
[12]A. Payne, N. Todd, E. Minalga, Y. Wang, M. Diakite, R. Hadley, R. Merrill, R. Factor, L. Neumayer, and D. L. Parker, "*In vivo* evaluation of a breast-specific magnetic resonance-guided focused ultrasound system in a goat udder model," Med. Phys. **40**, 073302 (9pp.) (2013).
[13]R. Deckers, L. G. Merckel, B. Denis de Senneville, G. Schubert, M. Köhler, F. M. Knuttel, W. P. T. M. Mali, C. T. W. Moonen, M. A. A. J. van den Bosch, and L. W. Bartels, "Performance analysis of a dedicated breast MR-HIFU system for tumor ablation in breast cancer patients," Phys. Med. Biol. **60**, 5527–5542 (2015).
[14]C. T. W. Moonen and C. Mougenot, "MRI-guided focused ultrasound, apparatus for novel treatment of breast cancer," in *Philips Research Book Series* (Springer, New York, NY, 2006), Vol. 6, pp. 183–200.
[15]C. Mougenot, M. Tillander, J. Koskela, M. O. Köhler, C. Moonen, and M. Ries, "High intensity focused ultrasound with large aperture transducers: A MRI based focal point correction for tissue heterogeneity," Med. Phys. **39**(4), 1936–1945 (2012).
[16]A. Payne, R. Merrill, E. Minalga, U. Vyas, J. de Bever, N. Todd, R. Hadley, E. Dumont, L. Neumayer, D. A. Christensen, R. B. Roemer, and D. L. Parker, "Design and characterization of a laterally mounted phased-array transducer breast-specific MRgHIFU device with integrated 11-channel receiver array," Med. Phys. **39**(3), 1552–1560 (2012).
[17]D. J. D'Orsi, E. A. Sickles, E. B. Mendelson, and E. A. Moris, *Breast Imaging Reporting and Data System: ACR BI-RADS—Breast Imaging Atlas*, 5th ed. (American College of Radiology, Reston, VA, 2013).
[18]E. R. Price, J. Hargreaves, J. A. Lipson, E. A. Sickles, R. J. Brenner, K. K. Lindfors, B. N. Joe, J. W. T. Leung, S. A. Feig, L. W. Bassett, H. Ojeda-Fournier, B. L. Daniel, A. W. Kurian, E. Love, L. Ryan, D. D. Walgenbach, and D. M. Ikeda, "The California breast density information group: A collaborative response to the issues of breast density, breast cancer risk, and breast density notification legislation," Radiology **269**(3), 887–892 (2013).
[19]Cancer.org BI-RADS categories, http://www.cancer.org/treatment/understandingyourdiagnosis/examsandtestdescriptions/mammogramsandotherbreastimagingprocedures/mammograms-and-other-breast-imaging-procedures-mammo-report, accessed on 12th August 2014.
[20]F. A. Duck, *Physical Properties of Tissues: A Comprehensive Reference Book* (Academic Press, London, UK, 1990), pp. 73–166.
[21]E. Minalga, A. Payne, R. Merrill, N. Todd, S. Vijayakumar, D. L. Parker, and R. Hadley, *Design and Evaluation of RF Coils for Magnetic Resonance Guided High Intensity Focused Ultrasound* (International Society of Magnetic Resonance in Medicine, Montreal, Canada, 2011), p. 1726.
[22]The Engineering Toolbox, http://www.engineeringtoolbox.com/thermal-conductivity-d_429.html, accessed on 16 August 2015.
[23]P. A. Hasgall, F. Di Gennaro, C. Baumgartner, E. Neufeld, M. C. Gosselin, D. Payne, A. Klingenböck, and N. Kuster, IT'IS Database for thermal and electromagnetic parameters of biological tissues, version 2.6, 13th January 2015, www.itis.ethz.ch/database, accessed on 12 August 2015.
[24]M. Malinen, T. Huttunen, J. P. Kaipio, and K. Hynynen, "Scanning path optimization for ultrasound surgery," Phys. Med. Biol. **50**, 3473–3490 (2005).
[25]AZO Materials, An AZO Network site, http://www.azom.com/properties.aspx?ArticleID=920, accessed on 16 August 2015.
[26]A. C. Kak and K. A. Dines, "Signal processing of broadband pulsed ultrasound: Measurement of attenuation of soft biological tissues," IEEE Trans. Biomed. Eng. **25**, 321–344 (1978).
[27]H. L. Le, "An investigation of pulse-timing techniques for broadband ultrasonic velocity determination in cancellous bone: A simulation study," Phys. Med. Biol. **43**, 2295–2308 (1998).
[28]U. Vyas and D. A. Christensen, "Ultrasound beam simulations in inhomogeneous tissue geometries using the hybrid angular spectrum method," IEEE Trans. Ultrason., Ferroelectr., Freq. Control **59**(6), 1093–1110 (2012).
[29]S. Almquist, J. T. de Bever, R. Merrill, D. L. Parker, and D. A. Christensen, "A full-wave phase aberration correction method for transcranial high-intensity focused ultrasound brain therapies," in *36th Annual International Conference of the IEEE Engineering in Medicine and Biology Society (EMBC), 26-30 August 2014* (IEEE, 2014), pp. 310–313.
[30]C. R. Dillon, A. Payne, D. A. Christensen, and R. B. Roemer, "The accuracy and precision of two non-invasive, magnetic resonance-guided focused ultrasound-based thermal diffusivity estimation methods," Int. J. Hyperthermia **30**(6), 362–371 (2014).
[31]H. H. Pennes, "Analysis of tissue and arterial blood temperatures in the resting human forearm," J. Appl. Physiol. **1**(2), 93–122 (1948).
[32]M. Malinen, T. Huttunen, K. Hynynen, and J. P. Kaipio, "Simulation study for thermal dose optimization in ultrasound surgery of the breast," Med. Phys. **31**(5), 1296–1307 (2004).
[33]S. A. Sapareto and W. C. Dewey, "Thermal dose determination in cancer therapy," Int. J. Radiat. Oncol., Biol., Phys. **10**(6), 787–800 (1984).
[34]B. E. Billard, K. Hynynen, and R. B. Roemer, "Effects of physical parameters on high temperature ultrasound hyperthermia," Ultrasound Med. Biol. **16**(4), 409–420 (1990).